Original scientific paper

Received: August 19, 2015
Accepted: March 7, 2016
DOI: 10.1515/rmzmag-2016-0003

Reconstruction and appraisal of Akunu–Akoko area iron ore deposits using geological and magnetic approaches

Raziskava in ocena železovega nahajališča na območju Akunu–Akoko z uporabo geoloških in magnetometrijskih metod

Cyril Okpoli*, Adedibu Akingboye
Department of Earth Sciences, Adekunle Ajasin University, Akungba–Akoko, Ondo State, Nigeria
*cyril.okpoli@aaua.edu.ng

Abstract

Geological mapping and magnetic methods were applied for the exploration of iron ore deposits in the Akunu–Akoko area of Southwestern Nigeria for the purpose of evaluating their geological characteristics and resource potentials. A proton magnetometer measures the vertical, horizontal and total magnetic intensities in gammas. The subsurface geology was interpreted qualitatively and quantitatively. The downward continuations and second vertical derivatives, the small-sized mineralised bodies and shallow features in the study area were mapped. The faults are trending in the following directions: NE–SW, NW–SE, N–S and E–W groups, while the iron ore mineralisation is structurally controlled by two major groups of fault trends, namely, the NE–SW and NW–SE; the N–S and E–W groups are mere occurrences that do not contribute to the structural control of the iron ore mineralisation in Akunu.

The upward continuation has a linear feature similar to the principal orientation of the regional faults, while Locations 2 and 3 have relatively high magnetic susceptibility zones; suspected to be iron ore deposits. The depths to the magnetic sources ranged from 25 m to about 250 m.

Key words: magnetic method, geological mapping, quantitative interpretation, Akunu, Nigeria

Izvleček

Z geološkim kartiranjem in magnetno metodo smo raziskali železovo nahajališče na območju Akunu–Akoko v jugozahodni Nigeriji z namenom, opredeliti njegove geološke značilnosti in surovinski potencial. S protonskim magnetometrom smo merili vertikalno, horizontalno in celotno magnetno intenziteto, izraženo v gamah. Opravljena je bila kvalitativna in kvantitativna geološka interpretacija območja nahajališča. Izvedli smo kartiranje nadaljevanja orudenja v globino, analizo drugega vertikalnega odvoda (Second Vertical Derivative, SVD) in kartiranje tudi manjših rudnih teles in geoloških značilnosti raziskovanega območja. Smeri glavnih prelomov so NE–SW, NW–SE, N–S in E–W. Zgradbo nahajališča določata dve glavni skupini prelomov smeri NE–SW in NW–SE, medtem ko tisti, ki potekajo v smereh N–S in E–W, na orudenost v Akunuju niso vplivali.

Nadaljevanje orudenosti navzgor se izraža z linearnim vzorcem, podobnim glavni usmerjenosti regionalnih prelomov, medtem ko razkrivata lokaciji 2 in 3 cone razmeroma visoke magnetne susceptibilnosti, ki utegnejo ustrezati telesom železove rude. Viri magnetnih anomalij so ugotovljeni med 25 m in približno 250 m globine.

Ključne besede: magnetna metoda, geološko kartiranje, kvantitativna interpretacija, Akunu, Nigerija

© 2016 Cyril Okpoli, published by De Gruyter Open.
This work is licensed under the Creative Commons Attribution-NonCommercial-NoDerivs 3.0 License.

Brought to you by | National & University Library
Authenticated
Download Date | 4/18/17 12:22 PM

Introduction

Inversion of potential field data can readily provide models of the distribution of physical properties in the subsurface, but rigorous geological interpretation of those property models is challenging. For mineral exploration, qualitative interpretations may be based on associations expected for mineralisation or alteration, such as the existence of 'coincident magnetic and density anomalies' [1–3].

Assumptions of remanent magnetisation can pose difficulty as it can be acquired at different stages in the history of the rock and rotated in subsequent tectonic events. Direct measurement of remanent magnetisation is also challenging as it requires multiple oriented samples to provide a representative estimate of the magnetisation of a complete rock mass. Li et al. [4], Telford et al. [5], and Medeiros and Silva [6] are among the seasoned authors who have addressed this challenge of estimating magnetisation direction from magnetic field data. In spite of these efforts, however, most magnetic field interpretations originate from the unqualified assumption that the effects of remanent magnetisation are insignificant. Only for anomalies that demonstrably cannot be caused by a feasible geology and an induced-only magnetisation is the presence of remanent magnetisation invoked. The nonuniqueness of potential field inversion permits remanent magnetisation to pass unnoticed in many magnetic field interpretations, with the consequence that estimates of magnetic parameters such as the shape, location and dip of source bodies are also in error. Helbig analysis [7–11] provides a direct method for the estimation of magnetisation direction from the magnetic field itself. It is therefore a desirable aspect of all magnetic field interpretations, if only to confirm that magnetic anomalies are indeed caused by a magnetisation parallel to the geomagnetic field.

There are variations in the composition of magnetic properties within a rock type [12] depending on chemical inhomogeneities, depositional and/or crystallisation conditions and postdeformational conditions, as well as their contributions in terms of mineral to the magnetic susceptibility of a rock [13–15]. The values of magnetic susceptibility depend on the grain size, the presence of minute crystal lattice defects, such as dislocations, lattice vacancies, impurities, etc. and the amount of iron ore in a sample. When the rocks are closely examined, they are found to be composed of discrete grains of different sizes, shapes and colours. These grains are minerals, which are the building blocks of all rocks [16]. The successful application of geophysical methods to iron ore exploration is based upon the existence of measurable physical contrast associated with it [17].

The magnetic method is a geophysical technique that measures variations in the earth's magnetic field to determine the location of subsurface features. This nondestructive technique has numerous applications in engineering and environmental studies, including the location of voids, near-surface faults, igneous dikes and buried ferromagnetic objects such as storage drums, pipes etc. [18]. Magnetic field variations can be interpreted to determine an anomaly's depth, geometry and magnetic susceptibility.

In this study, ground magnetic data of the Akunu–Akoko iron ore deposit is analysed and interpreted with the objective of delineating its concealed iron ore bodies, as well as mapping the lithologic contacts, depth to magnetic sources and basement structures. In addition, the petrographic studies of the rocks are analysed to determine and know the mineral counts present in each rock sample collected from the field during geological mapping of the study area through petrographic study of the thin section under plane- and cross-polarised light in order to know which mineral actually undergoes oxidation and reduction during the mineralisation of the iron ore.

Geological settings, rock types and structures

Akunu–Akoko is located in Akoko North West Local Government area of Ondo State, Southwestern Nigeria, and lies within the basement complex of Nigeria. The area lies within latitudes 7°35'N–7°40'N and longitudes 5°55'E–5°60'E (Figure 1).

The Precambrian rocks of Nigeria may be grouped into three principal subdivisions.

Brought to you by | National University Library
Authenticated
Download Date | 4/18/17 12:22 PM

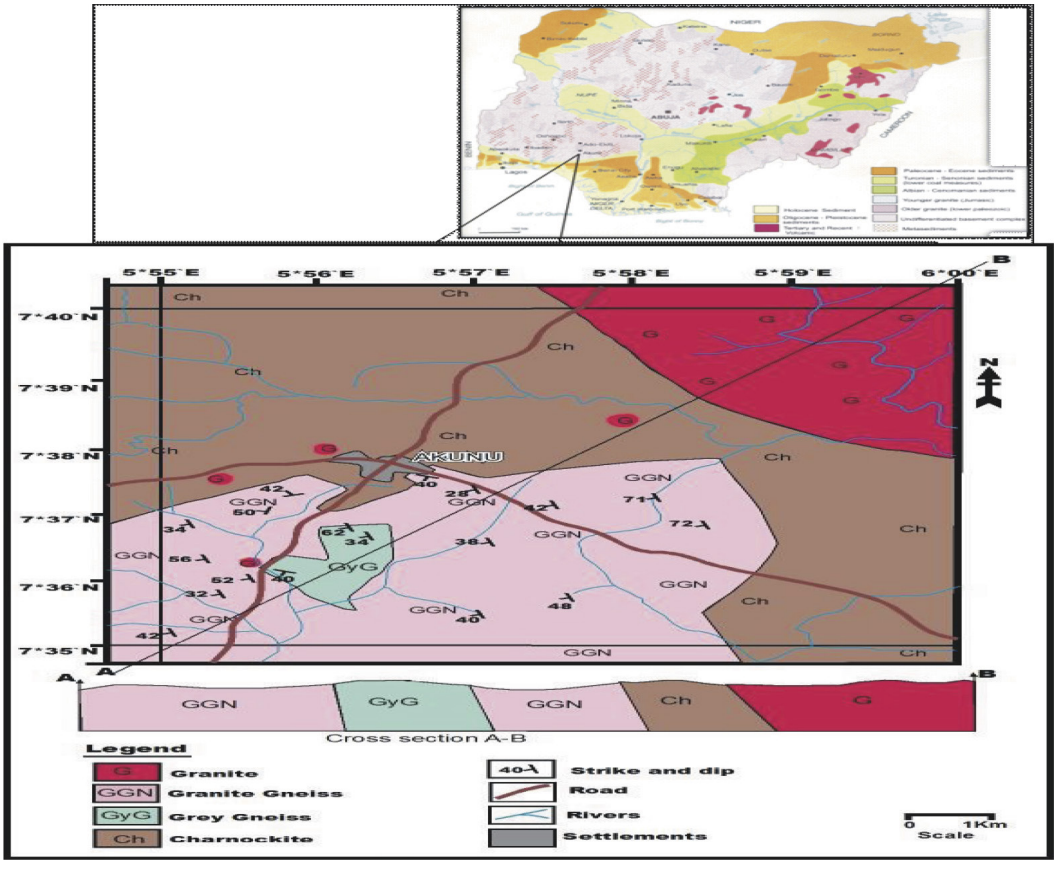

Figure 1: *Geological map of the study area.*

These are the ancient gneiss migmatite complex, the schist belts and the plutonic series, plus affiliated minor rocks, which bear imprints of Liberian (~2700 Ma), Eburnean (~2000 Ma) and Pan-African (~ 650 Ma) tectonic events, the latter being the most widespread. Older ages >3.0 Ga have more recently been indicated for some. Such relict signatures tend to reinforce the assertion that this Precambrian terrain may have been part of an Archean protoshield, which was later affected by Proterozoic crustal activities and subsequent evolution of the Phanerozoic basins. Overlying these older assemblages are sedimentary sequences of the Cretaceous-to-Tertiary ages deposited in five basins [19, 20].

Akunu–Akoko lies within the basement complex of Nigeria and is underlain by Southwestern Nigeria's basement complex rocks. The area is situated in the predrift mobile belt east of the West African and Sao Luis cratons and Northeast of the Congo craton, which were affected by the Pan-African orogeny (ca. 600 Ma). The entire belt lies in the reactivated region that resulted from plate collision between the West African Craton and the active Pharusian continental margin [21–23].

The geological history of the area is similar to the structural evolutions that had affected the basement complex of Nigeria. The rocks present in the area include migmatites, granite, charnockite, granite gneiss and other felsic and mafic intrusives. From these lithological units and the geological map of the area produced during the course of the exercise, different theories can be advanced for the geological history of the area. It could be inferred that the granite gneiss is the oldest because it was derived from the metamorphism of granite, followed closely by granite and lastly by charnockites (Figure 1). The granite was later emplaced but has not been metamorphosed; hence, it is younger than the granite gneiss. The charnockitic rocks were later emplaced by stopping or metasomatism. This seems to be the most plausible explanation for the origin of the Akunu charnockites.

Brought to you by | National Chiao Tung University Library
Authenticated
Download Date | 4/18/17 12:22 PM

Table 1: *Mineral composition in various rock types.*

Sample no	Name of rock sample	Quartz	Microcline	Plagioclase	Biotite	Hornblende	Opaque
LOC3	Granite gneiss	38.4	16.5	27.3	10.0	6.6	1.2
LOC3B	Granite gneiss	30.9	12.6	42.9	8.6	4.2	0.8
LOC4	Granite	38.6	18.6	22.9	13.2	5.5	1.2
LOC5	Granite	34.4	20.4	27.5	12.6	4.5	0.6
LOC9	Charnockite	21.4	37.2	32.1	6.5	1.1	2.1
LOC10	Charnockite	20.4	38.4	31.3	5.1	3.4	1.4
LOC11	Charnockite	18.4	40.0	29.9	9.6	TR	2.1
LOC12	Charnockite	19.6	39.4	28.4	7.4	4.4	0.8
LOC13	Charnockite	20.0	40.1	32.4	4.5	2.1	0.9

The crystalline rocks were later intruded by pegmatite and aplites after the emplacement of charnockites.

The rocks in the study area are divided structurally into two, which are fault and fold. Faults were seen on some of the rocks, but the displacements were not too pronounced; however, in the case of the latter, the folds were pronounced. Chiefly, all types of folds were seen on the outcrops; some were even refolded as a result of episodes of orogeny.

Materials and methods

Microscopic description and trace mineral identification

We took measurements of the strike and dip of the exposed rocks, and samples were taken for petrographic studies in the laboratory.

Petrographic studies of each of the rock units were carried out during the course of this research. This was done by observing thin sections of some of the representative samples under reflected light. The minerals were identified using their optical properties such as colour, form, relief, cleavage, birefringence, pleochroism, extinction and twinning. Modal analysis was done using visual estimation of the proportions of minerals in the rocks through a chart produced by Terry and Chilinger [24].

The study revealed that the nine rock samples taken during the research on field are of the following types: five samples of charnockite, two samples of granite gneiss and two samples of granite, all made up of essentially microcline, plagioclase, quartz, biotite and orthoclase feldspar with microcline and opaque minerals (Table 1).

Principle and measurement of magnetic susceptibility

Magnetic susceptibility is the degree of magnetisation of a material in response to an applied magnetic field. The volume magnetic susceptibility, represented by the symbol K, is defined by the following relationship [25]:

$$M = KH \tag{1}$$

where M is the magnetisation of the material (the magnetic dipole moment per unit volume), measured in amperes per metre, and H is the applied field, also measured in amperes per metre (Eq. 1). Both quantities are measured in Système International (SI) units.

The magnetic induction B is related to H by the relationship:

$$B = \mu_0(H + M) = (1 + K)\,\mu_0 H = \mu H \tag{2}$$

where μ_0 is the permeability of free space ($4\pi \times 10^{-7}$Henry/m) and is the relative permeability of the material (Eq. 2).

If K is positive, then $(1 + K) = >1$, and the material is called paramagnetic. In this case, the magnetic field is strengthened by the presence of the material. Alternatively, if K is negative, then $(1 + K)$ is <1, and the material is diamagnetic. As a result, the magnetic field is weakened in the presence of the material.

Brought to you by | National University Library
Authenticated
Download Date | 4/18/17 12:22 PM

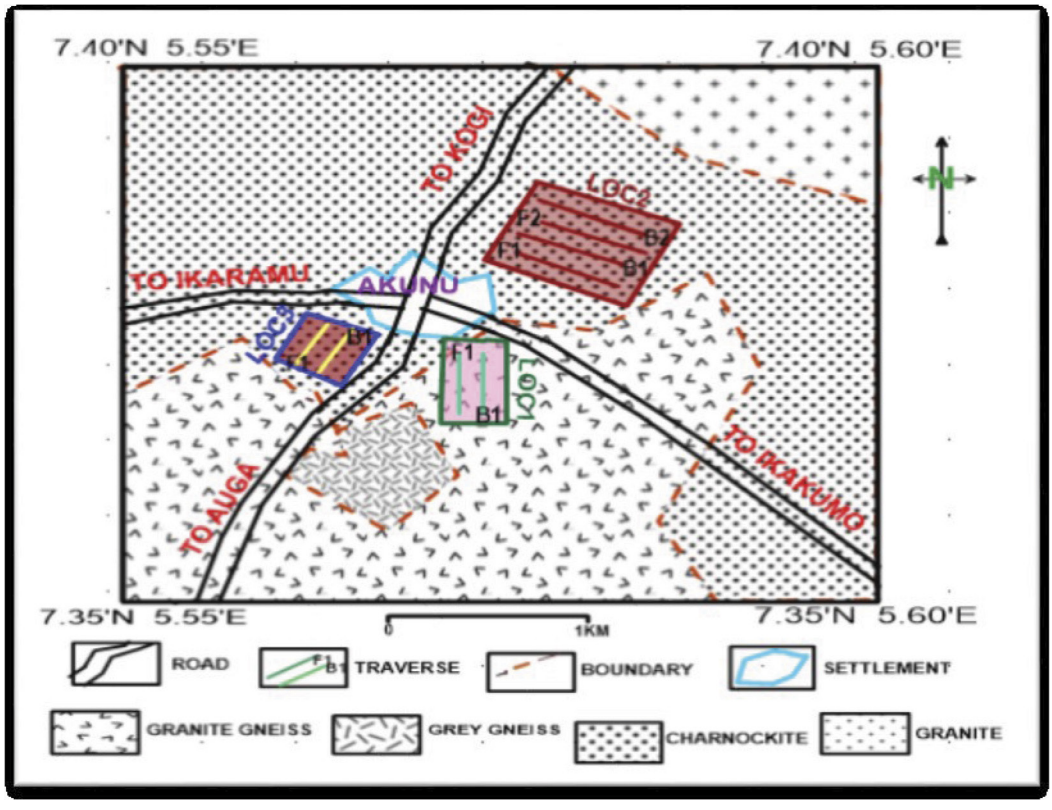

Figure 2: *Data acquisition map of the study area.*

Ground magnetic measurements and processing

The magnetic measurements in the survey area were made with a GSM-19T proton precession magnetometer; the equipment measures three components, which are the vertical, horizontal and total magnetic intensities, in gammas (nanoteslas, nTs). The magnetic profiling of the base and mobile stations was carried out with GSM-19T proton precession magnetometer at the three locations (Figure 2) around and over the buried granite gneiss (Location 1) along two traverses, which lie within latitudes 7°37'20.00^{2}N–7°37'37.00^{2}N and longitudes 5°56'26.00^{2}E–5°56'50.30^{2}E, covering a distance of 800 m, respectively, only to know the range of the magnetic intensity and the fracturing density system of the rock. The suspected iron ore /charnockite sites (Location 2) along four traverses lie within latitudes 7°38'01.60^{2}N–7°38'05.98^{2}N and longitudes 5°56'57.70^{2}E–5°58'61.98^{2}E, covering a distance of 1 km each, and the charnockitic gneiss (Location 3) along two traverses lies within latitudes 7°37'40.20^{2}N–7°38'26.33^{2}N and longitude 5°56'11.98^{2}E–5°56'20.45^{2}E, covering a distance of 400 m each. Observations were made along the series of traverses at three locations at equal spacing of 20 m, with a base station carefully selected, where the magnetic intensities are being measured at a stationary point. The magnetic data collected in the study area were processed so as to prepare the data set for interpretations by applying diurnal correction to remove the effect of diurnal variation. The magnetic measurement grid was closed by establishing base measurement points outside each profile; repeat magnetic readings were taken at these survey points before and after measurements were made at Locations 1, 2 and 3, respectively (Figure 2). This was done with the purpose of carrying out drift and/or diurnal corrections on the magnetic data recorded. The variation of earth's magnetic field with time, which may last several hours to 1 day, is called diurnal variation [26]. The detected diurnal variation was removed from our data of the observed drift in the magnetic reading. Five repeat magnetic readings and time observations were inputted at 20 m intervals along

Brought to you by | National Chiao Tung University Library
Authenticated
Download Date | 4/18/17 12:22 PM

each profile. In order to remove magnetic noise and diurnal magnetic variation from the data obtained, the magnetic data were filtered using a three-point moving technique [26, 27]. Noise due to secular variation was considered very negligible because the measurement time was <2 hours for each profile line. After the diurnal correction and filtering were carried out, the next stage of magnetic reduction was to calculate the anomalous geomagnetic field. The earth's normal magnetic field was calculated through International Geomagnetic Reference Field (the known regional geomagnetic field of 32,000 nT for Akunu area) and subtracted from the diurnal-corrected observed value to produce the residual geomagnetic field. The corrected geomagnetic field data are presented as profiles for the six profiles (Figure 2). The anomalous geomagnetic field data were plotted on the vertical axis, and the station position on the horizontal axis. Both qualitative and quantitative interpretations of the reduced geomagnetic field were subsequently carried out. The accuracy of the proton precession magnetometer reading is ±1 nT, while that of the reduced anomalies is ±5 nT.

We used Oasis Montaj software for the quantitative interpretation of the magnetic profiles. The total magnetic intensity (TMI) and fast Fourier transform (FFT) maps from the magnetic data were modelled through various analyses to improve their quality for better understanding of the subsurface geology of the deposit. The desired improvements on the quality of the ground magnetic data were achieved by the application of two-dimensional FFT filters using reduction to poles, second vertical derivatives (SVDs), upward and downward continuations, susceptibilities and power spectrum.

Mathematically, according to Dobrin and Savit [28], the Fourier transform of a space domain function *f(x, y)* is defined as follows:

$$F(\mu, V) = \iint f(x, y).e^{-t(\mu x + vy)}dxdy \qquad (3)$$

And its reciprocal relation is given as follows:

$$f(x, y) = \iint F(u, v).e^{t(\mu x + vy)}d\mu dv \qquad (4)$$

where μ and *v* are wave numbers in the *x*- and *y*-directions, respectively, measured in radians per metre, i.e., when x and y are in units of metres, these relate to spatial 'frequencies' *fx* and *fy* (in cycles per metre) (Eqs. 3 and 4).

The upward continuation filter allows the transformation of data measured on one surface to some higher surface [29] and tends to smooth the original data by attenuating short-wavelength anomalies relative to their long-wavelength counterparts. According to Trompat et al. [30], the downward continuation filter when applied to potential field data brings the observation surface closer to the source, therefore enhancing the responses from sources at depth. The SVD is applied to the magnetic data to enhance local anomalies obscured by broader regional trends. It accentuates short-wavelength components of the anomaly field, while deemphasising long-wavelength components. The susceptibility filter computes the apparent magnetic susceptibility of magnetic sources, with certain assumptions applied, viz., (i) that the IGRF has been removed from the data; (ii) that no remanent magnetisation exists; and (iii) that all magnetic response is caused by a collection of vertical prisms of infinite depth and strike extent [31].

Reduction to the pole is used in low magnetic latitudes to change an anomaly to its equivalent as would be observed at the north magnetic pole. This transformation simplifies the interpretation and visualisation of anomalies from low magnetic latitudes.

The reduction to pole is carried out as follows [32]:

$$(\theta) = (1/sinIa + i\,cosI.cos(D - \theta)) \qquad (5)$$

where

I geomagnetic inclination

I_a inclination for amplitude correction (never less than I)

D geomagnetic declination

When reducing to the pole from equatorial latitudes, North–South features can be blown up due to the strong amplitude correction (the *sin(I)* term) that is applied when $(D - \theta)$ is p/2 (i.e., a magnetic east–west wavenumber) (Eq. 5). By specifying higher latitudes for the amplitude correction alone, this problem can be reduced or eliminated at the expense of undercorrecting the amplitudes of North–South features. An amplitude inclination of 90 causes only the phase component to be applied to the

Brought to you by | National University Library
Authenticated
Download Date | 4/18/17 12:22 PM

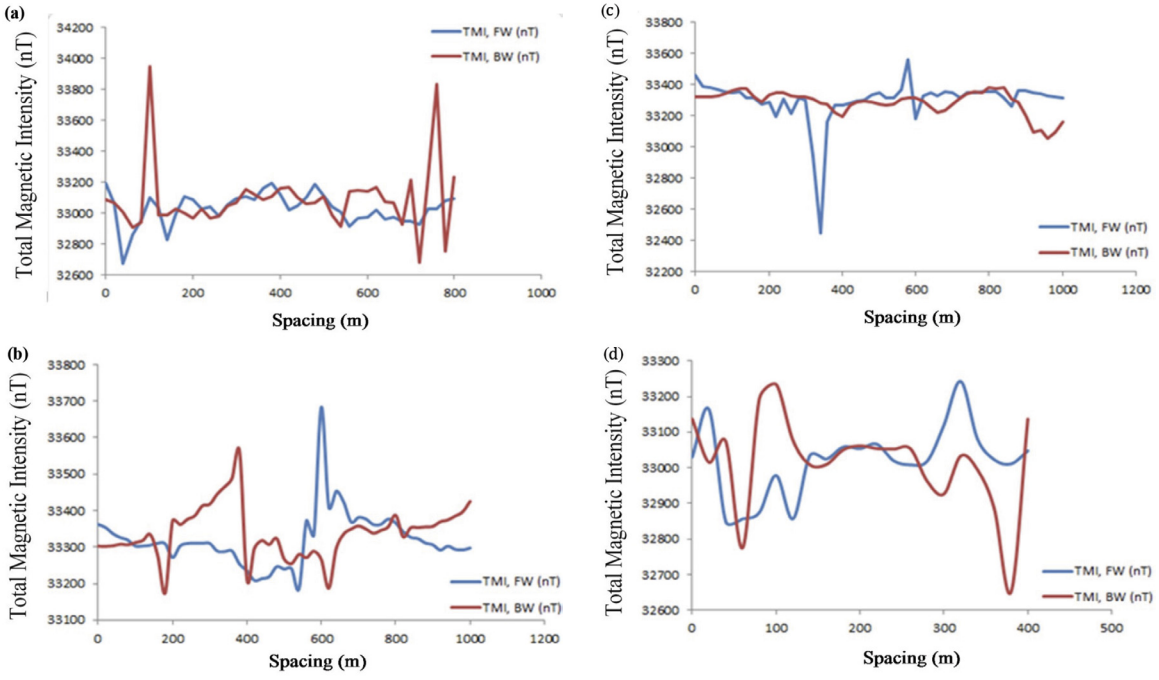

Figure 3: *(a) Magnetic intensity profile of Location 1, (b) magnetic intensity profile of Location 2 Traverse 1, (c) magnetic intensity profile of Location 2 Traverse 2 and (d) magnetic intensity profile of Location 3*

data (no amplitude correction), and a value of zero causes phase and amplitude corrections to be applied over the entire range.

The spectral (harmonic) analysis of potential field data, which serves as an approximate guide in estimating the depth of magnetic source, was also carried out. Figure 11 shows the radial averaged spectrum of the ground magnetic data and the depth estimate plot of its analysis.

Results and discussion

Qualitative interpretation of magnetic data

The main use of magnetic profiles or maps and their derivatives in mineral prospecting is to make geological deductions from them. From the range of magnetic intensity values of these data, information on subsurface lithology, trend and geological structures can be obtained [28].

The profile of Location 1 (Figure 3a) was only plotted to know the range of the magnetic intensity in order to give a clue to the fracturing density of the rock. The backward (BW) traverse shows high magnetic intensities of 33,000–33,900 nT between the distance of 220 m and 1,000 m, respectively, which represent undeformed granite gneiss, while the gentle low amplitude of magnetic intensities ranging from 32,640 nT (700 m) to 32,980 nT (200 m) represent deformed granite gneisses; moreover, there are traces of iron ore within the host rock due to the low magnetic intensities and susceptibility of the rocks. These were also seen in the forward (FW) traverse of the survey area, with very low magnetic intensities ranging from 32,620 nT (60 m) to 32,850 nT (720 m), which are more pronounced than in the BW traverse. The FW traverse also shows high magnetic intensities ranging from 33,080 nT (800 m) to 33,200 nT (0 m). The rocks also have little traces of mineralisation.

In the profile of Location 2 Traverse 1 (Figure 3b), the FW_1 to BW_1 stretch of the survey traverse has very distinctive low- and high-amplitude magnetic intensities ranging from 33,160–33,680 nT, respectively, and the total distance covered 1,000 m.

The BW traverse shows high magnetic intensities of 33,390 nT–33,400 nT between the distances of 480 m and 1,000 m, respectively, with gentle low amplitude of magnetic intensities ranging from 33,160 nT (160 m) to 33,350 nT (240 m), which represent deformed charnockitic rocks (i.e., weathered and fractured). The

Brought to you by | National Chung Hsing University Library
Authenticated
Download Date | 4/18/17 12:22 PM

FW traverse shows low magnetic intensities ranging from 33,160 nT (160 m) to 33,480 nT (520 m), with high magnetic intensities ranging from 33,680 nT (600 m) to 33,300 nT (920 m).
The profile of Location 2 Traverse 2 (Figure 3c) shows the FW_2 to BW_2 stretch of the survey traverses to have very distinctive low- and high-amplitude magnetic intensities ranging from 32,420 nT to 33,580 nT, respectively, and the total distance covered 1,000 m.
The BW traverse shows high magnetic intensities of 33,280–33,400 nT between the distances of 340 m and 800 m, respectively, and gentle low amplitude of magnetic intensities ranging from 33,000 nT (940 m) to 33,360 nT (200 m), which indicate deformed charnockitic rock. The FW traverse shows very low magnetic intensities ranging from 32,420 nT (340 m) to 33,360 nT (680 m), with high magnetic intensities ranging from 33,580 nT (600 m) to 33,300 nT (180 m). The total magnetic intensity of Traverse 2 is lesser than that of Traverse 1. The highs show that the charnockitic rocks have undergone no/less deformation, while the lows show that the rocks have become weathered and fractured (faults, joints) as a result of tectonic activities in the area. The geological structures constitute the bulk deposit of iron ore due to the low magnetic intensities and susceptibilities of the rocks. There is a major, more pronounced deep-seated fault showing up on the FW traverse.
The profile of Location 3 (Figure 3d) also showed that the magnetic intensities were distributed with very distinctive low- and very high-amplitude magnetic intensities ranging from 33,280 nT to 33,580 nT, respectively, and the total distance covered 400 m.
The BW traverse shows high magnetic intensities of 33,280–33,040 nT between the distances of 100 m and 320 m, respectively, showing low amplitude of magnetic intensities ranging from 32,640 nT (380 m) to 33,020 nT (40 m). These are also seen in the FW traverse of the survey area, with very low magnetic intensities ranging from 32,840 nT (40 m) to 33,040 nT (200 m) and high magnetic intensities ranging from 32,960 nT (100 m) to 33,280 nT (340 m). The fracturing system constitutes iron ore mineralisation due to the low magnetic intensities and susceptibilities of the rocks, but in minute amounts, not even up to one-tenth of Location 2, which is the main deposit of the iron ore.
The FW and BW profiles were combined to produce the shaded colour in the TMI maps for Location 2 Traverse 1 (Figure 4a), Location 2 Traverse 2 (Figure 4b) and Location 3 (Figure 4c) of the Akunu–Akoko area, respectively.
Location 2 is the area where the iron ore mineralisation is suspected to have occurred. Traverse 1 (Figure 4a) showed that the magnetic signature regions (A, B and G) of this map were characterised by relatively high magnetic intensity values (7.061–57.528 nT), dominantly seen in the northwestern, northeastern and a small portion of the southwestern parts on the TMI map, with the southwestern, northwestern and a small portion of the northeastern parts of the area (C, D and E) having relatively low magnetic intensity values (-162.160 nT to 0.001 nT).
Traverse 2 (Figure 4b) showed magnetic signature regions (A, B and H) of relatively high magnetic intensity values (10.056–30.211 nT) dominantly seen towards some part of eastern and western parts of the study area, while the southern, northern and a small portion of the northwestern part of the area (D, G and I) had relatively low magnetic intensity values (-18.582 nT to 0.838 nT). The relatively high magnetic intensity could be the result of the presence of charnockites, which is the most widespread rock in the area. These observations compared favourably well with the geologic map (Figure 1). The relatively low magnetic intensity coincides with the presence of weathered/fractured rocks and (E) the iron ore mineralisation.
The TMI map of Location 3 (Figure 4c) ranges in amplitude from -308.532 nT to 47.716 nT, suggesting contrasting rock types in the basement of the study area. The regions A, B and C of this map are characterised by relatively high magnetic intensity values (13.555–47.716 nT), dominantly seen towards the northern and central portions of the map, which coincides with charnockitic gneiss on the surface geological map, while the southwestern part and a small portion of the northeastern part of the area with relatively low magnetic intensity values (-308.532 nT to 2.827 nT) coincides with the iron ore mineralisation.

Brought to you by | National and University Library
Authenticated
Download Date | 4/18/17 12:22 PM

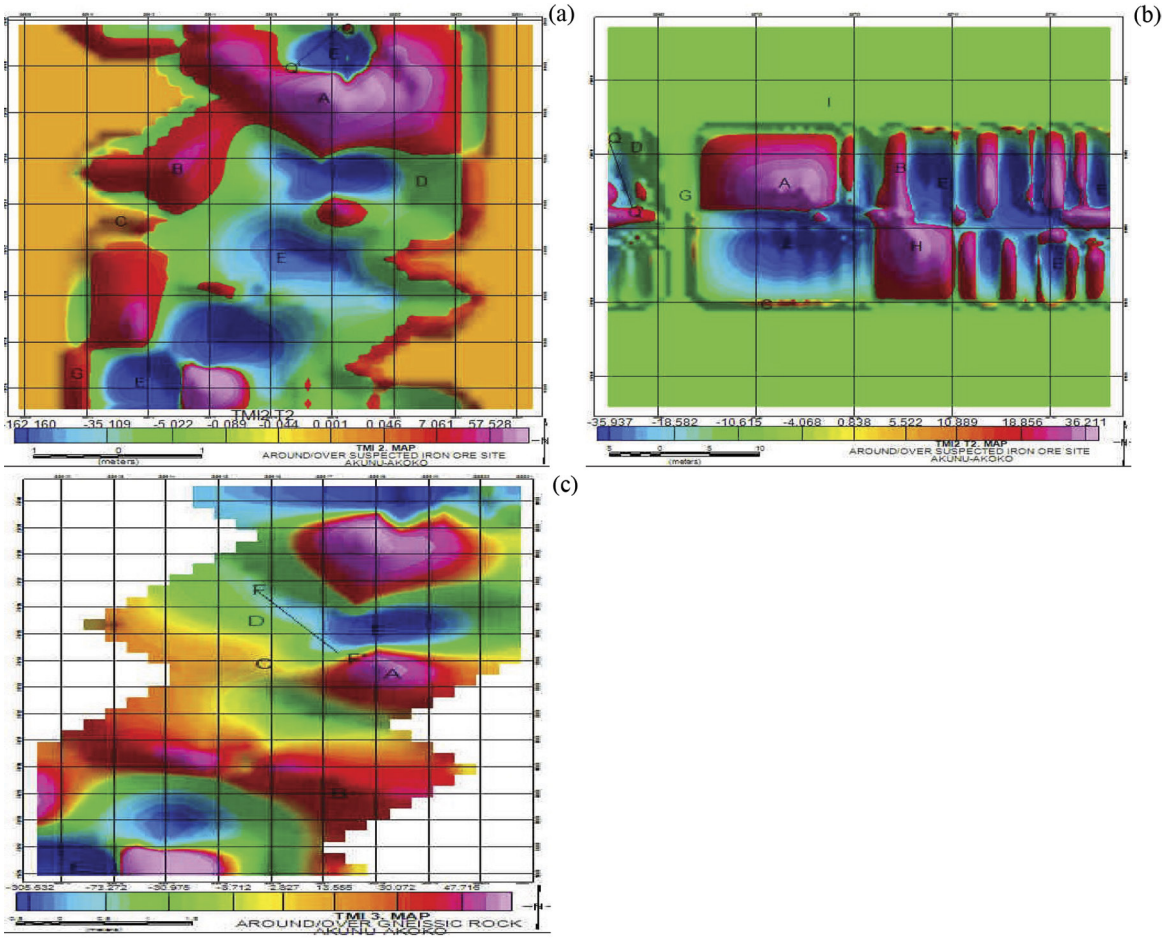

Figure 4(a, b and c): *Shaded colour ground magnetic map at Akunu–Akoko showing prominent anomalies marked A–E and G.*

The areas marked NE–SW (Q–Q') in Figure 4a, NW–SE (Q–Q') in Figure 4b and NW–SE (F–F') in Figure 4c are low-amplitude lineament anomalies, which may represent fault or fracture zones.

Figure 4 shows the combination signals of regional, residual and noise data; however, with the help of matched filtering, separation of signals was made possible, as can be seen from Figures 5–9.

The FW and BW profiles were combined to produce the shaded colour TMI maps for Location 2 Traverse 1 (Figure 4a), Location 2 Traverse 2 (Figure 4b) and Location 3 (Figure 4c) of the Akunu–Akoko area.

The FW and BW profiles were combined to produce the shaded colour TMI maps for Location 2 Traverse 1 (Figure 4a), Location 2 Traverse 2 (Figure 4b) and Location 3 (Figure 4c) of the Akunu–Akoko area.

Location 2 is the area where the iron ore mineralisation is suspected to have occurred. Traverse 1 (Figure 4a) showed magnetic signature regions (A, B and G) that are characterised by relatively high magnetic intensity values (7.061–57.528 nT), dominantly seen in northwestern, northeastern and a small portion of the southwestern areas of the TMI map, while the southwestern, northwestern and a small portion of the northeastern part of the area (C, D and E) had relatively low magnetic intensity values (–162.160 nTto 0.001 nT).

Traverse 2 (Figure 4b) showed magnetic signature regions (A, B and H) of relatively high magnetic intensity values (10.056–30.211 nT), dominantly seen towards some parts of eastern and western parts of the study area. The southern, northern and a small portion of the northwestern part of the area (D, G and I) had relative low magnetic intensity values (-18.582 nT to 0.838 nT). The relatively high magnetic intensity could be the result of presence of charnockites, which is the most widespread rock in the area. These compared favourably well with

Brought to you by | National Library
Authenticated
Download Date | 4/18/17 12:22 PM

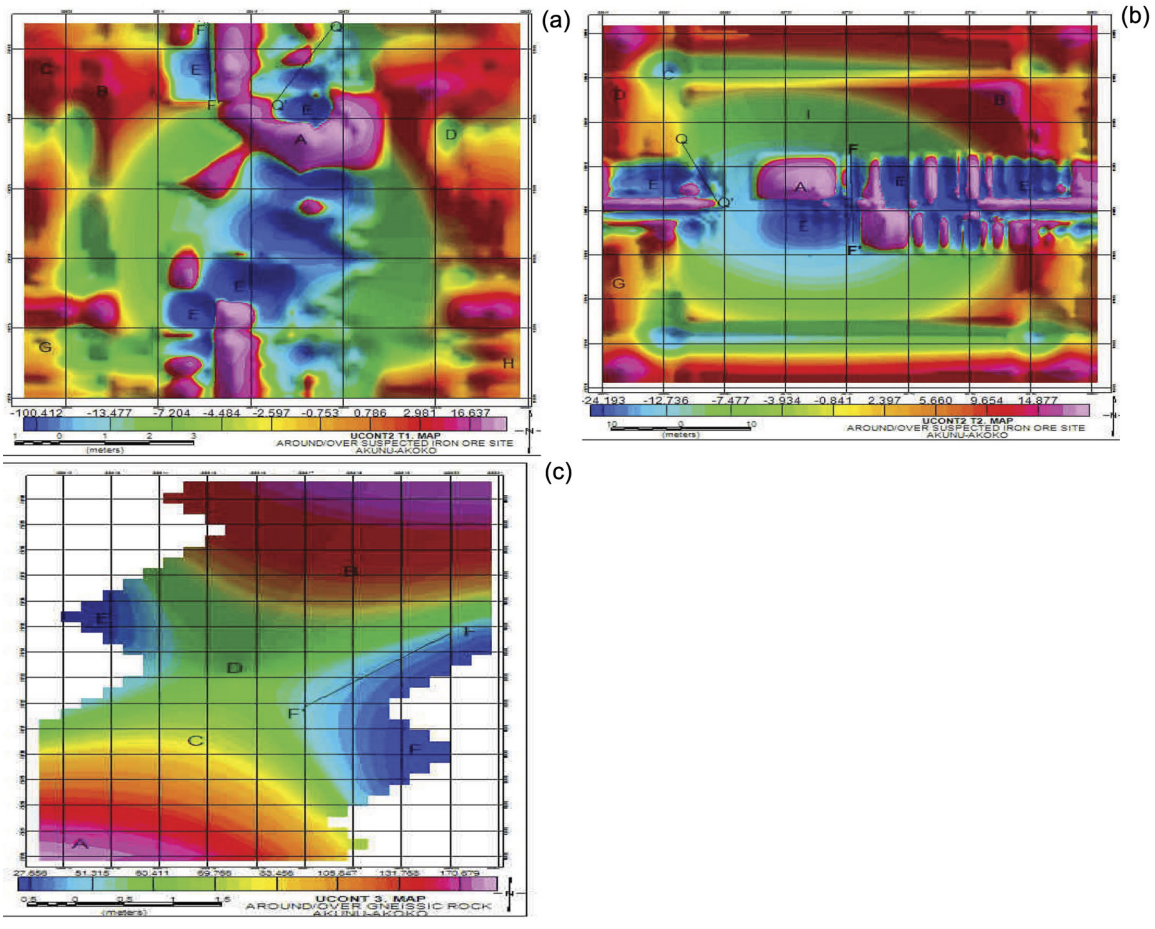

Figure 5(a, b and c): *The upward continuation filtered magnetic maps of Location 2 Traverses 1 and 2, as well as Location 3 of the study area, respectively.*

the geologic map (Figure 1). The relatively low magnetic intensity coincides with the presence of weathered/fractured rocks and (E) the iron ore mineralisation.

The TMI map of Location 3 (Figure 4c) ranges in amplitude from (-308.532 nT to 47.716 nT), suggesting contrasting rock types in the basement of the study area. The regions A, B and C of this map are characterised by relatively high magnetic intensity values (13.555 nT–47.716 nT), dominantly seen towards the northern and central portions of the map, which coincides with the presence of charnockitic gneiss on the surface geological map, while the southwestern and a small portion of the northeastern part of the area had relatively low magnetic intensity values (-308.532 nT to 2.827 nT) coinciding with the iron ore mineralisation.

The areas marked NE–SW (Q–Q') in Figure 4a, NW–SE (Q–Q') in Figure 4b and NW–SE (F–F') in Figure 4c indicate low-amplitude lineament anomaly, which may represent the fault or fracture zone.

Figure 4 shows the combination signals of regional, residual and noise data; however, with the help of matched filtering, separation of signals was made possible, as can be seen from Figures 5–9 respectively.

Figure 5a–c shows the upward continuation (UCONT) colour-shaded relief maps of Location 2 Traverses 1 and 2, as well as Location 3, of the study area respectively. The anomaly patterns identified in this map are a qualitative representation of the spatial variation in the magnetic properties of deep basement rocks and structures in the area. There is a good correlation in the trend of the low-amplitude magnetic anomalies (E) in Figure 5b with those of the iron ore zone (Figure 5b), except the outcrops trending towards the northern and the western parts on the map, which were obscured by near-surface

Brought to you by | National University Library
Authenticated
Download Date | 4/18/17 12:22 PM

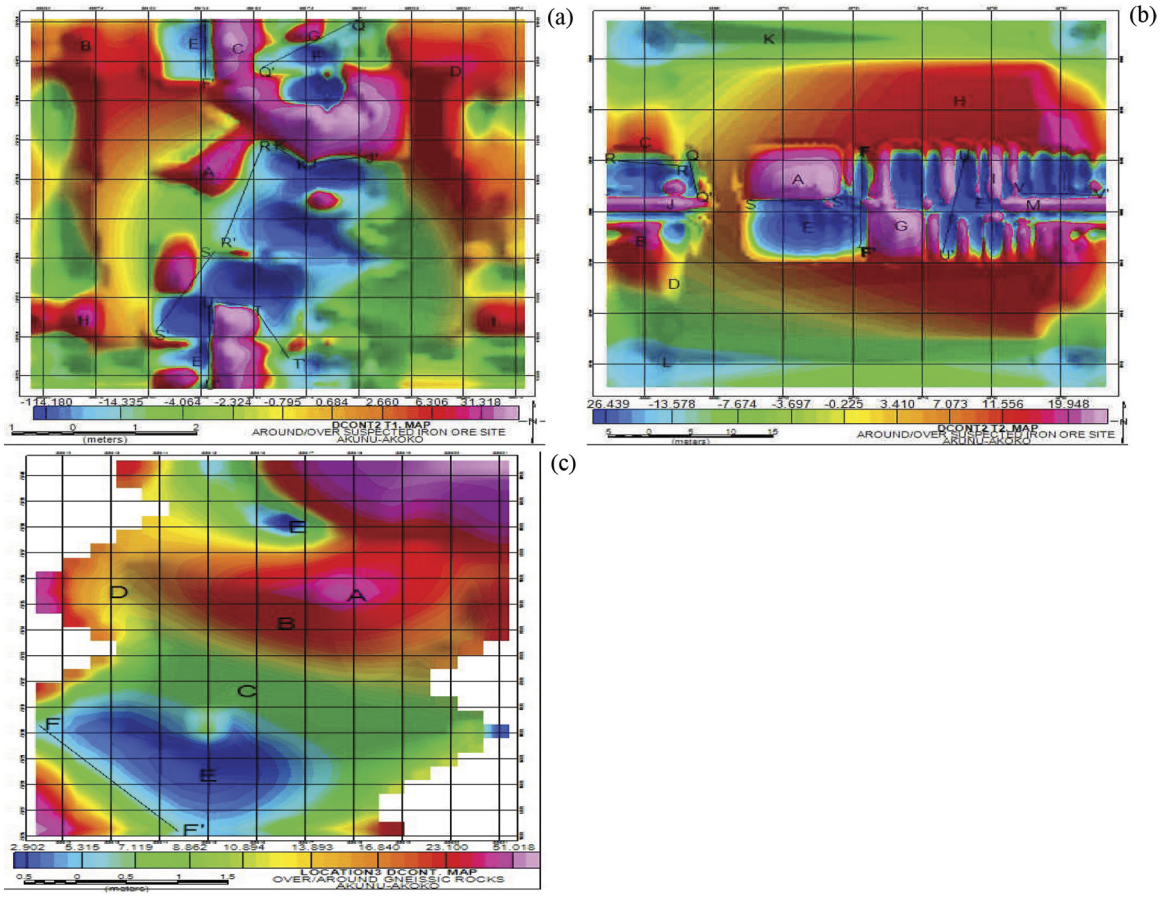

Figure 6(a, b and c): *The downward continuation map of Location 2 Traverses 1 and 2, as well as Location 3 (A–E) are small-sized mineralised bodies and F–F' is the inferred faulted zone).*

features of the outcrops of the region (B–D, and G) and the northern region (E) iron ore zone on the map. Furthermore, a NE–SW linear anomaly (Figure 5a) and NW–SE linear anomaly (Figure 5b) with amplitude range between -12.726 nT and 3.934 nT were delineated as deep-seated faults. In addition, an inferred fault F–F' is seen running North–South in the area (Figure 5b).

Figure 5c shows no good correlation in the trend of the low-amplitude magnetic anomalies (E) in Figure 4c with those of the central and the northern iron ore zones on the map. The NW–SE linear anomaly with amplitude range between -72.272 nT and -30.978 nT is delineated as deep-seated fault because it is continuous on both maps.

Consequently, this map is better for studying geologic features related to regional factors in the area.

Figure 6a–c are the downward continuation (DCONT) maps of Location 2 Traverses 1 and 2, as well as Location 3 of the study area, respectively. The DCONT Map (Figure 6) enables the easy observation of short-wavelength anomalies not seen in the original TMI map, marked A–E, G–K and M due to small-sized mineralised bodies in the study area.

Three of the short-wavelength high-amplitude anomalies, A, H and I (Figure 6a), have no similar trend (approximately East–West) with the prominent anomalies B, C and D (6.306–31.318 nT). In Figure 6b, four of the short-wavelength high-amplitude anomalies A, G, J and M have no similar trend (approximately East–West) with prominent anomalies B, C and D (-0.225 nT to 11.556 nT), whereas in Figure 6c, three of the short-wavelength high-amplitude anomalies G, H and L have a similar trend (approximately North–South) with prominent anomalies A, B and C (8.862–51.018 nT). These zones were identified as charnockitic gneissic rocks because of their correlation with the geological map. Areas with sharp change in magnetic intensity from high-amplitude anomaly

Brought to you by | National Chiao Tung University Library
Authenticated
Download Date | 4/18/17 12:22 PM

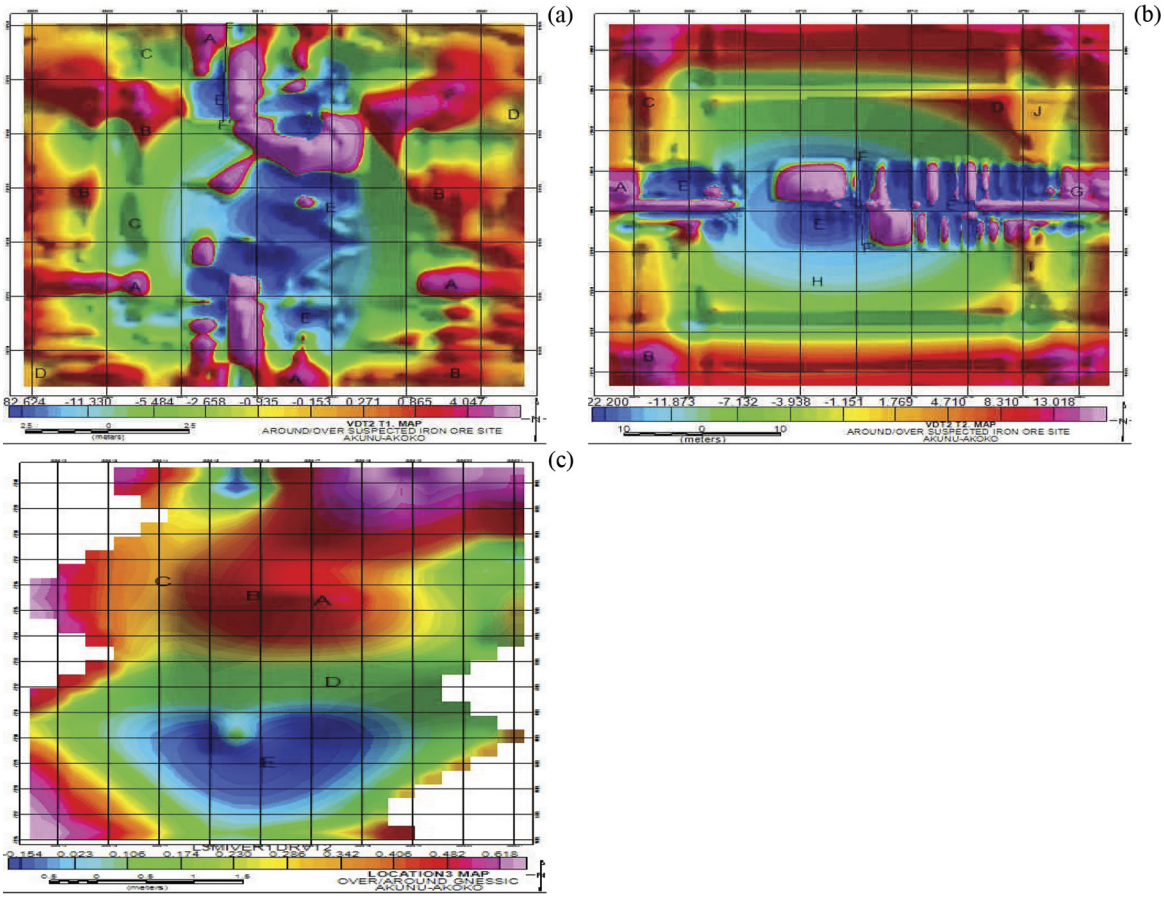

Figure 7(a, b and c): *SVD maps of Location 2 Traverses 1 and 2, as well as Location 3, respectively.*

to low-amplitude anomaly exhibited as narrow boundaries are inferred to be fault zones.

Faults were delineated and grouped into four types based on their trend, i.e., NE–SW group (J–J', R–R', S–S' and U–U'), E–W group (V–V'), N–S group (U–U') and NW–SE group (F–F', K–K', Q–Q' and T–T'), but F–F' and Q–Q' (Figure 6) are deep-seated faults. The iron ore mineralisation is structurally controlled by two major groups of fault trends, which are the NE–SW and the NW–SE, while other groups (N–S and E–W) are mere occurrences that did not contribute to the structural control of the iron ore mineralisation in the study area. The NE–SW faults are observed to correlate with the surface-mapped faults. The downward continuation map shows that both low- and high-magnetic intensity anomaly patterns characterise the study area and that the tectonic framework of the area is contributed mainly by faults.

Figure 7a–c are the SVD maps of Location 2 Traverses 1 and 2, as well as Location 3, of the study area, respectively. Figure 7 helps to highlight details and breaks in the anomaly texture of near-surface rocks, i.e., subtle, local and short-wavelength anomalies are emphasised. The short-wavelength anomalies marked A–E, I and J on this map are caused by near-surface small-sized mineralised bodies and/or geological features. The reason why these anomalies are not seen in the original TMI map is because they have been obscured by the stronger effect of the broader regional features in the area.

The north–south-trending, elongated, low-magnetic intensity anomaly marked F–F' at the north–southern edge of the map is identified as a possible fault zone.

Figure 8a–c shows the reduction to magnetic pole maps of Location 2 Traverses 1 and 2, as well as Location 3, of the study area, respectively. Reduction to magnetic pole (Figure 8) was used in low-amplitude magnetic latitudes to change an anomaly to its equivalent, as would be observed at the north magnetic pole. The

Brought to you by | National Library
Authenticated
Download Date | 4/18/17 12:22 PM

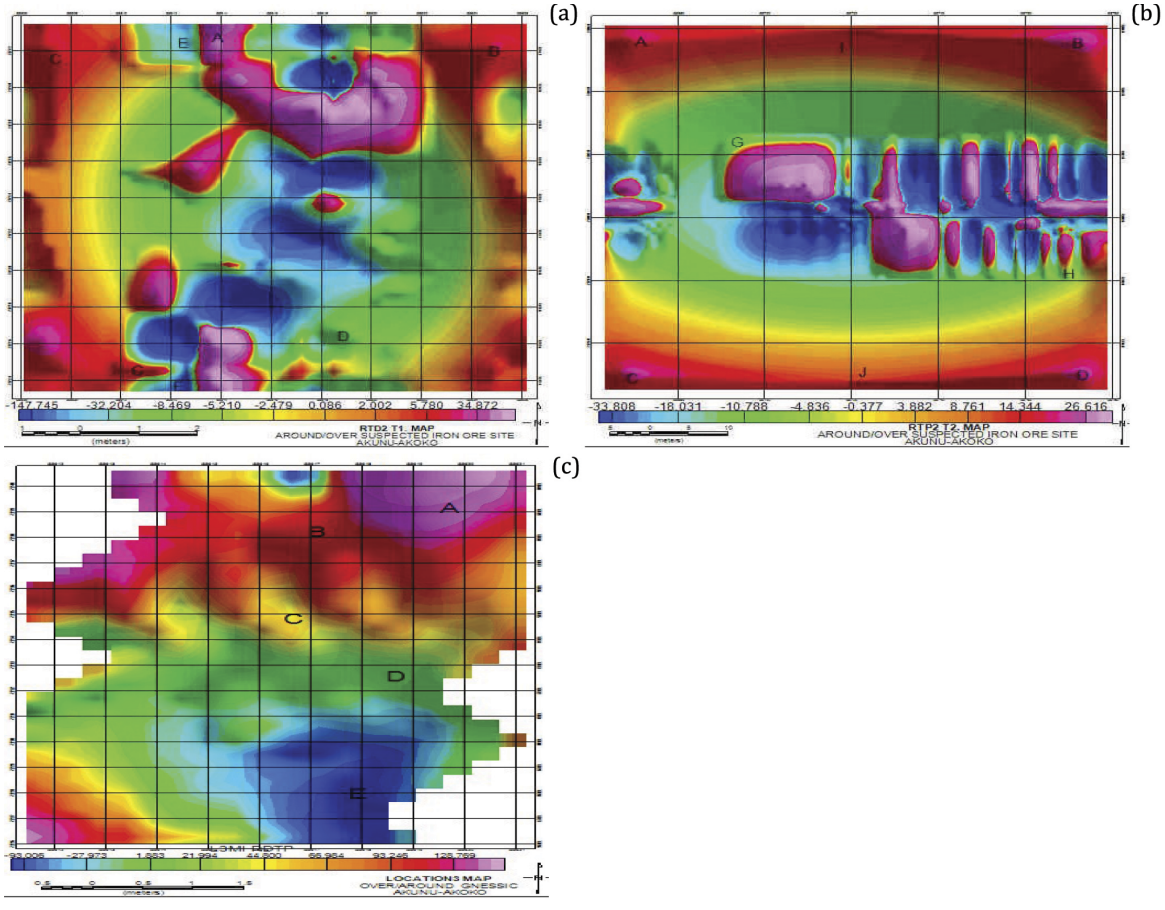

Figure 8(a, b and c): *The reduction to pole maps of Location 2 Traverses 1 and 2, as well as Location 3.*

areas marked A, B, C, D, G, I and J are areas in low magnetic latitudes and were transformed to enable better visualisation at the northern section of the map. The points marked A, B, C, I, and J (Figure 8b) are seen more clearly towards the Northern and Southern poles, compared to the other filtered maps produced for Location 2 Traverse 2. These regions showed that weathered/fractured structure and iron ore mineralisation are included in the charnockitic rocks. The point marked E (Figure 8c) is more seen clearly towards the southern pole.

Figure 9a–c are the susceptibility maps of Location 2 Traverses 1 and 2, as well as Location 3, of the study area, respectively. The apparent susceptibility map (Figure 9) was used to define the magnetisation domains within the study area, and rock types were inferred based on the range of susceptibility values within these domains. In Figure 9a, relatively high magnetic susceptible zones (1.289–5.537 nT) could be inferred as areas where the iron ores are concentrated in the deposit and low susceptible zones (-95.183 nT to -2.743 nT) as areas with charnockite or charnockitic rocks. In Figure 9b, relatively high magnetic susceptible zones (9.726–17.324 nT) could also be inferred as areas where the iron ores are concentrated in the deposit and low susceptible zones (-18.532 nT to -3.894 nT) as areas with charnockite rocks.

Figure 10a and b are the radial spectrum and depth estimate plots of Locations 2 and 3, respectively. The depths to the top of the geologic sources that produced the observed anomalies in the magnetic map were determined using spectral analysis. The radially average power spectrum in the study area ground magnetic data shows a normal plot that has straight line segments that decrease in slope with increasing frequency. From the radially average power spectrum depth estimate curve in Figure 10, the depths to the magnetic sources in the area ranged from 25 m to 250 m.

Brought to you by | National Library
Authenticated
Download Date | 4/18/17 12:22 PM

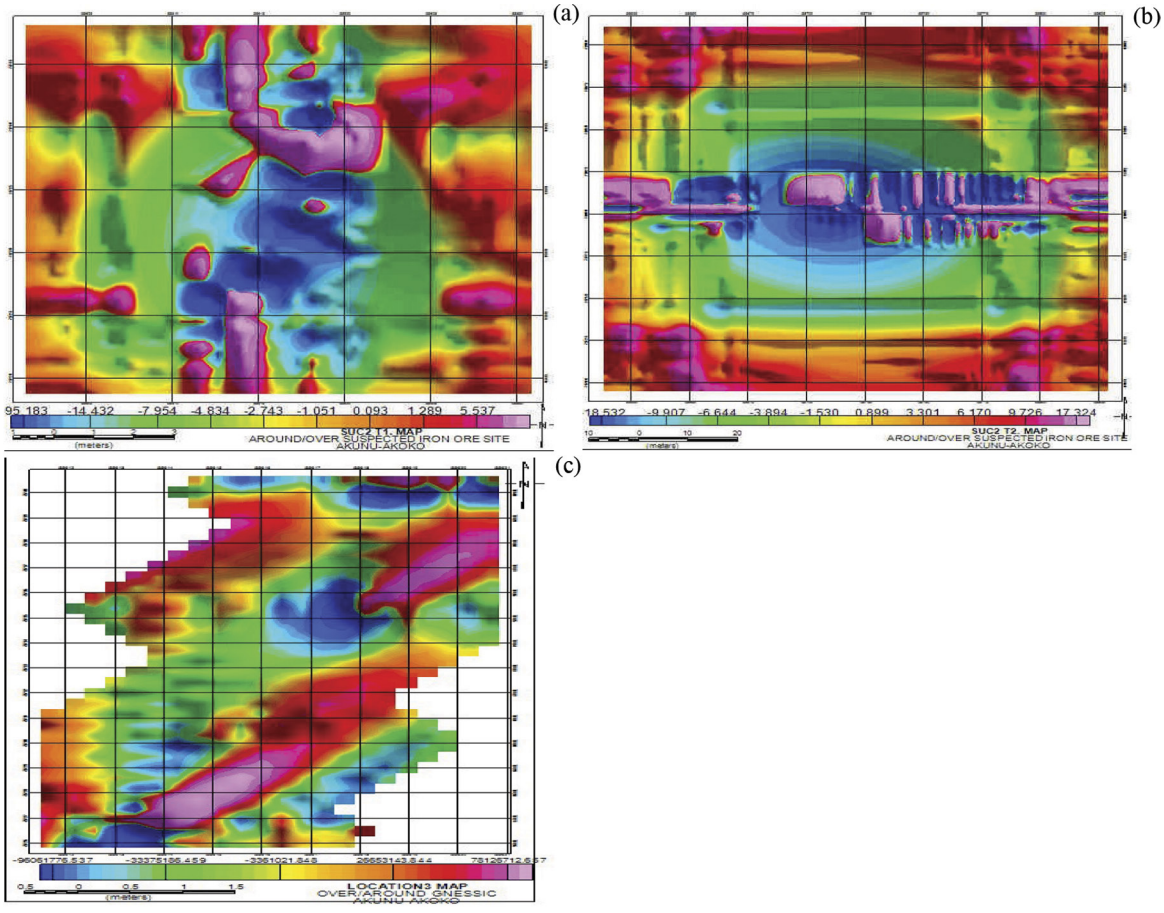

Figure 9(a, b and c): *The apparent susceptibility maps of the ground magnetic data showing the distribution of magnetisation domains within Location 2 Traverses 1 and 2, as well as Location 3.*

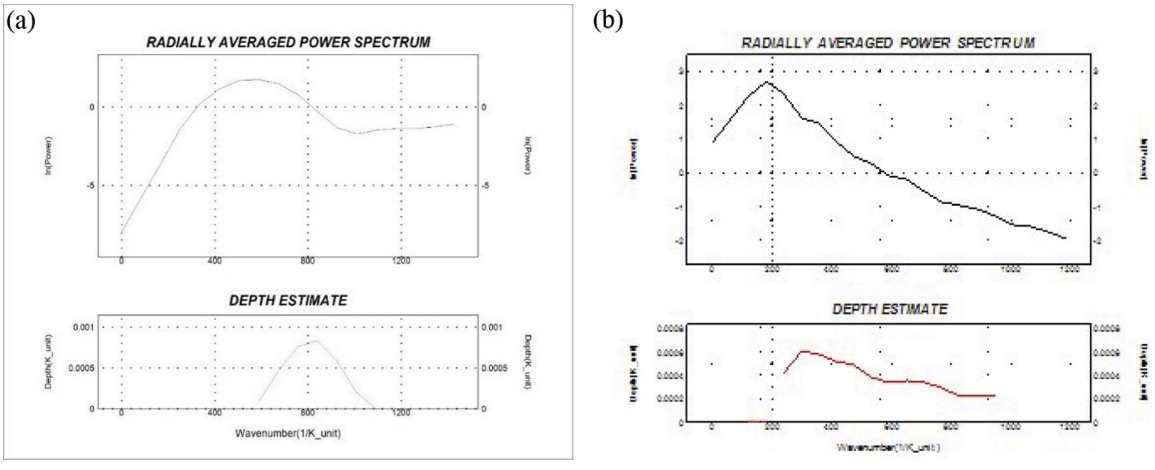

Figure 10(a and b): *The radial spectrum and depth estimate plot of Locations 2 and 3, respectively.*

Brought to you by | National University Library
Authenticated
Download Date | 4/18/17 12:22 PM

LOC 3B LOC4 LOC5

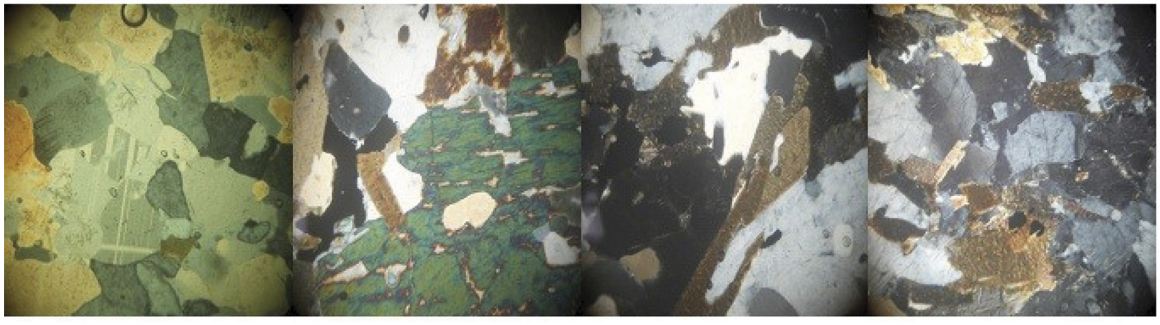

LOC 9 LOC 10 LOC 11 LOC 12 LOC 13

Figure 11: *Photomicrographs of thin sections of rock samples under plane-polarised light (PPL) granite gneiss (3, 3B), granite (4, 5) and charnockite (9, 10, 11, 12, 13).*

LOC 3 LOC 3B LOC 4 LOC 5

LOC 9 LOC 10 LOC 11 LOC 12 LOC 13

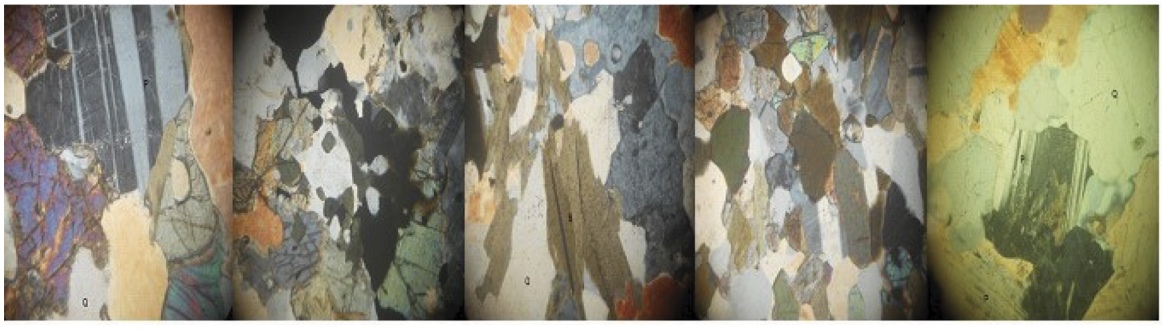

Figure 12: *Photomicrographs of thin sections of rock samples under cross-polarised light/crossed Nicol (XPL) granite gneiss (3, 3B), granite (4, 5) and charnockite (9, 10, 11, 12, 13).*

Brought to you by | National Chiao Tung University Library
Authenticated
Download Date | 4/18/17 12:22 PM

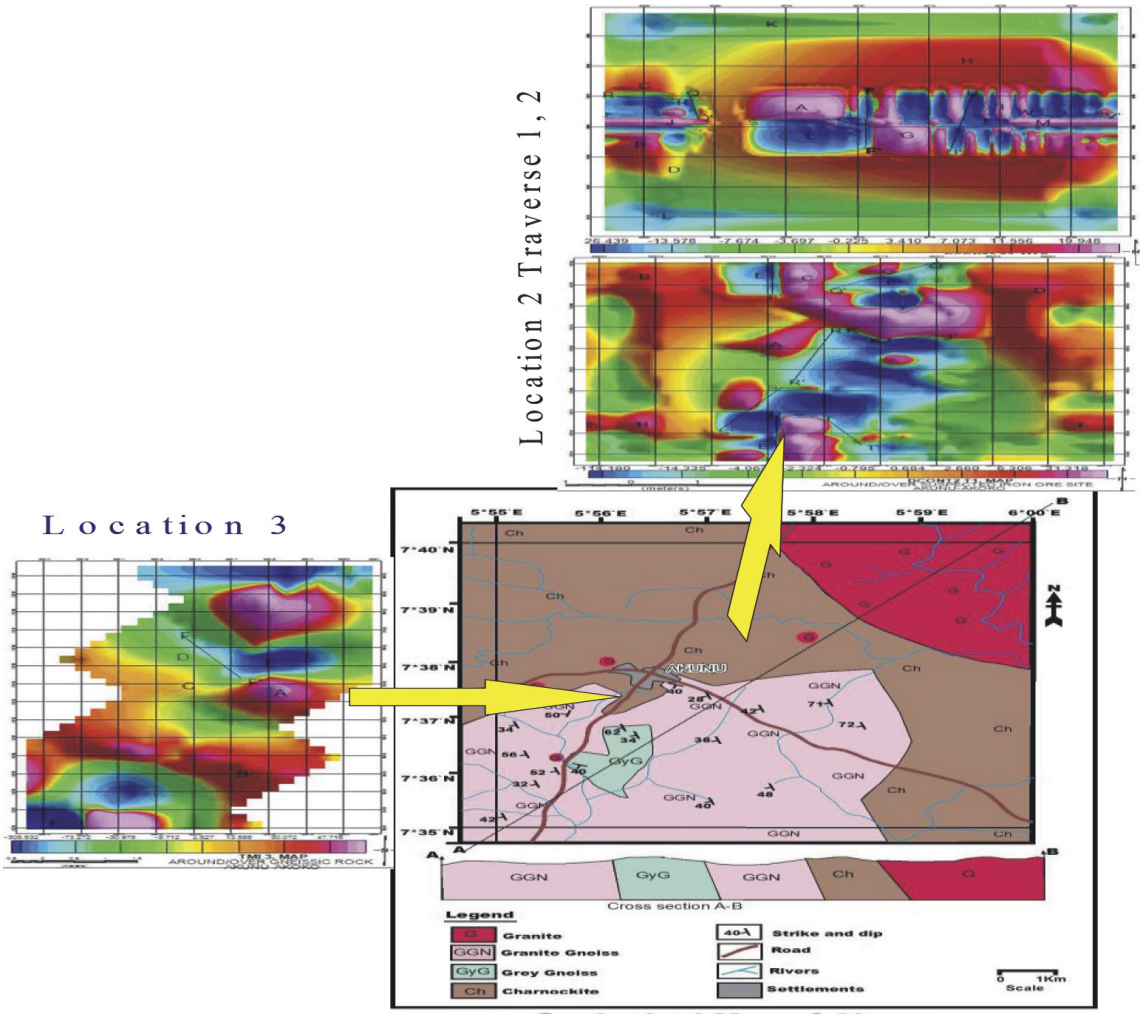

Figure 13: *Modified geologic map of the study area [33].*

Thin section and microscopic interpretation of the rock samples

Figures 11 and 12 show the results of photomicrographs of the various rock types studied under crossed and plane-polarised light. The minerals present are plagioclase ($Na(AlSi_3O_8$-$Ca(Al_2Si)O_8)$), which is a colourless mineral in thin section. It occurs as a plate or lath-shaped section. It is characterised by an imperfect cleavage. Relief is low and birefringence is weak, with interference colours that are pale yellow of the first order. Maximum extinction varies, and polysynthetic twinning is common in the mineral, according to albeit law. Orthopyroxene (hypersthene H, $[Mg,Fe]SiO_3$) is the common mineral usually observed in charnockitic rocks; its colour is greyish white or yellowish. Low birefringence first-order colour, usually first-order yellow or lower, is the characteristic features of this mineral when viewed under a petrological microscope. Orthopyroxene is highly pleochroic and pale coloured in thin section, with subtle pinkish-to-greenish pleochroism. It changes from pale green to pale pink when rotated on the stage. Orthopyroxene is distinguished from clinopyroxene by lower birefringence, parallel extinction and the common pale pink-to-green pleochroism. Despite its low abundance, hypersthene (a calcium-poor, iron-rich pyroxene) is a distinctive feature of this rock. Quartz, Q (SiO_2), mineral is colourless in thin section and occurs as euhedral prismatic crystals, as observed in Figures 11 and 12. It is characterised by the absence of cleavage; however, cleavage substances showed up on the edge of the slide. Relief of the mineral is low and it has a weak birefringence, thus showing as a maximum first-order

Brought to you by | National University Library
Authenticated
Download Date | 4/18/17 12:22 PM

Table 2: *Part of result of the derivative computation of Akunu–Akoko iron ore deposit (Location 2 Traverse 1).*

EASTING(X)	NORTHING(Y)	TMI,Z(nT)	RTP	DCONT	UCONT	SUC	VDT
55657.7	73801.61	33361.95	33706.46	33455.78	33337.65	0.16	0.24
55660	73801.61	33353.46	33712.06	33412.2	33333.65	0.16	0.14
55662.5	73801.61	33336.46	33715.11	33368.57	33329.58	0.16	0.05
55664.45	73801.61	33325.89	33716.48	33326.42	33325.51	0.16	-0.04
55666.55	73801.61	33319.07	33717.04	33287.25	33321.49	0.16	-0.13
55668.5	73801.61	33302.89	33717.67	33252.58	33317.58	0.16	-0.2
55670.45	73801.61	33303.1	33719.23	33223.93	33313.82	0.16	-0.25
55672.55	73801.61	33304.97	33722.59	33202.82	33310.27	0.16	-0.28
55674.5	73801.61	33310.46	33728.64	33190.76	33306.99	0.16	-0.29
55676.45	73801.61	33309.24	33738.23	33189.27	33304.04	0.16	-0.27
55678.55	73801.61	33271.67	33752.21	33199.8	33301.45	0.16	-0.22
55680.5	73801.61	33302.87	33769.99	33221.33	33299.21	0.16	-0.14
55682.45	73802.58	33309.94	33789.18	33249.71	33297.15	0.16	-0.03
55684.55	73802.58	33310.77	33807.28	33280.58	33295.12	0.16	0.07
55686.5	73802.58	33310.39	33821.79	33309.61	33292.97	0.16	0.18
55688.55	73802.58	33310.29	33830.22	33332.44	33290.53	0.16	0.27
55690.5	73802.58	33289.07	33830.05	33344.71	33287.67	0.16	0.33
55692.45	73802.58	33287.69	33818.78	33342.07	33284.21	0.16	0.35

white interference colour. Extinction is parallel in euhedral crystals and symmetrical to cleavage traces. Twining is absent in thin sections of the mineral. It is ubiquitous in all the samples analysed. Biotite ($K(Mg,Fe)_2(AlSi_3)O_{10}(OH)_2$) ranges from brown to yellowish brown to reddish brown as observed under thin section. The mineral is pleochroic, occurring as a plate and laths showing mineral stretching lineation on a microscopic scale. Cleavage is perfect in one direction; but sections cut parallel do not show cleavage. Polysynthetic twinning also occurs in some crystals, and the mineral occurs in minor amounts in all the samples. Extinction is usually parallel to the cleavage traces, which intersect at 90°. Moreover, hornblende ($NaCa_2(Mg,Fe)_4AlSi_6Al_2O_{22}(OH,F)_2$) mineral occurs in the rocks. It is pleochroic in various shades of green and brown in plane-polarised light. Hornblende ranges from yellow to green to dark brown, while the opaque minerals (zircon) appear black under plane-polarised light and crossed Nicol as studied under thin section. The evidence of the occurrence of the iron ore in the charnockites (Figure 3A–E) is seen from the decrease in the percentage of plagioclase feldspar present and the amount of microcline present in them, which are not supposed to be so if compared with the gneissic rocks (1A–2B) in the study area. This is a good evidence to prove the iron ore mineralisation zones. Moreover, when related to the interpretations of the ground magnetics of maps produced, good derivation could be made.

Figure 13 shows the reconstructed map of the study area, which revealed the correlation of the detailed geological mapping and two-dimensional inversion of the magnetic data. The charnockites and granites rock in the study area host high magnetic susceptibility and remanence. Moreover, the rocks are structurally controlled in the magnetisation and hosting of the ore mineral.

Conclusion

On the basis of the results of this geophysical interpretation, the distribution of the concealed iron ore bodies in the Akunu–Akoko

Brought to you by | National Chiao Tung University Library
Authenticated
Download Date | 4/18/17 12:22 PM

area, the range of depth to magnetic sources, the lithologic contacts and basement structures were established. The maps showed the spatial distribution of iron ore mineralisation in Location 3 and bulk deposit of this iron ore mineralisation in Location 2, and mere traces in Location 1 (composed of granite gneiss) because the fracturing density system of granite gneiss is low compared to the regions with bulk deposit (Location 2), which is made up of charnockitic rocks, with respective magnetic intensities for the host rocks, weathered/fractured zone and faults in the study area. The comparison of the geologic map (Figure 1) with the total magnetic ground maps of the selected locations produced show that the geological structures host the iron ore mineralisation in the host rocks (granite gneiss and charnockite), and this revealed more detailed geological information of the study area. These modifications are evidenced in the lithologic boundaries and mapping of more faults, predominantly those with no surface expression.

The trend pattern of the iron ore mineralisation shows that the rock is structurally controlled vis-a-viz trending approximately northeast–southwest in the south and east–west in the central area and north–south in the northern section of the maps, but structurally controlled by two major groups of fault trends, which are the NE–SW and the NW–SE, while other groups (N–S and E–W) are mere occurrences that do not contribute to the structural control of the iron ore mineralisation in the study area.

The mapping exercise has been able to reveal the general geology of the study area. In addition, the photomicrographs have shown various minerals present in rock types (containing quartz, feldspar and biotite, with some orthopyroxene, typically hypersthene) in the study area and those that could have originated from the formation of the iron ore.

References

[1] Henkel, H. (1976): Studies of density and magnetic properties of rocks from northern Sweden: *Pure and Applied Geophysics*, 114, 235–249.

[2] Puranen, R. (1989): Susceptibilities, iron and magnetite content of Precambrian rocks in Finland: *Tutkimusraportti – GeologianTutkimuskeskus – Report of Investigation* – Geological Survey of Finland.

[3] Henkel, H. (1994): Standard diagrams of magnetic properties and density; a tool for understanding magnetic petrology: *Journal of Applied Geophysics*, 32, 43–53.

[4] Li, Y., Shearer, S., Haney, M., Dannemiller, N. (2004): Comprehensive approaches to the inversion of magnetic data with strong remanent magnetization, *74th Ann. Internat. Mtg., Soc. Explor. Geophys.*, Expanded Abstracts.

[5] Telford, W. M., Geldart, L. P., Sheriff, R. G., Keys, D. A. (1976): *Applied Geophysics*: Cambridge University Press, Cambridge, pp. 7–215, 632–692.

[6] Medeiros, W. E., Silva, J. B. C. (1995): Simultaneous estimation of total magnetization direction and spatial orientation: *Geophysics*, 50, 1365–1377.

[7] Helbig, K. (1963): Some integrals of magnetic anomalies and their relation to the parameters of the disturbing body: *Zeitschrift für Geophysik*, 29, 83–96.

[8] Valyashko, G. M., Ivanenko, A. N., Czerniawski, G. E., Lukyanov, S. V. (1995): Interpretation procedure of marine magnetic data: topical problems. In: Gorodnitsky, A. M. (Ed.): *Anomalous Magnetic Field of the World Ocean*, CRC Press, Boca Raton, Florida, pp. 21–66.

[9] Schmidt, P. W., Clark, D. A. (1997): Directions of magnetization and vector anomalies derived from total field surveys: *Preview*, 70, 30–32.

[10] Schmidt, P. W., Clark, D. A. (1998): The calculation of magnetic components and moments from TMI: a case study from the Tuckers igneous complex, Queensland: *Exploration Geophysics*, 29, 609–614.

[11] Phillips, J. D. (2005): Can we estimate magnetization directions from aeromagnetic data using Helbig's integrals? *Earth, Planets and Space*, 57, 681–689.

[12] Carmichael, R. S. (1989): *Practical Handbook of Physical Properties of Rocks and Minerals*: CRC Press, Boca Raton, Ann Arbor, Boston.

[13] Thompson, R., Oldfield, F. (1986): *Environmental Magnetism*: Allen and Unwin, London, 227 pp.

[14] Lowrie, W. (1990): *Fundamental of Geophysics*, Low Price Paper Back Edition: Cambridge University Press, Cambridge, pp. 229–306.

[15] Schon, J. H. (1996): Physical properties of rocks: fundamentals and principle of petrophysics. In: Klaus, H., Sven, T. (Eds): *Handbook of Geophysical Exploration*, Vol. 18, Pergamon Press, London, 583 p.

[16] Mazzullo, J. (1996): *Investigations into Physical Geology, A Laboratory Manual*: Saunders College Publishing, New York, 361 p.

Brought to you by | National and University Library
Authenticated
Download Date | 4/18/17 12:22 PM

[17] Weymouth, J. W. (1985): *Geophysical Surveying of Archaeological Sites Surveying*: Archaeological Geology Yale University Press, New Haven and London, pp. 191–235.

[18] Rahaman, M. A. (1976): *A Review of the Basement Geology of Southwestern Nigeria*: Elizabeth Publishing Co., Nigeria, pp. 41–58.

[19] Ajayi, T. R. (1981): Ground magnetic studies of Ilesa east Southwest Nigeria: *African Journal of Environmental Science and Technology*, 4(3), 122–131.

[20] Burke, K. C., Dewey, J. F. (1972): Orogeny in Africa. In: Dessauvagie, T. F. J., Whiteman, A. J. (Eds): *African Geology*, University of Ibadan, Nigeria, pp. 583–608.

[21] Black, R., Caby, R., MonssinePouchkin, A., Bayer, R., Betrand, J. M., Boullier, A. M., Fabre, J., Lesquer, A. (1979): Evidence for late Precambrian plate tectonics in West Africa: *Nature*, 278, 223–227.

[22] Caby, R., Bertrand, J. M., Black, R. (1981): Pan-African closure and Continental collision in the Hoggar-Iforas segment central Sahara. In: Kroner A. (Ed): *Precambrian Plate Tectonics*, Elsevier, Amsterdam, pp. 407–434.

[23] Terry, Chilinger, J. S. P. (1955): Chart for visual estimation of percentage of minerals in rocks.

[24] Kearey, P., Brooks, M., Hill, I. (2002): *An Introduction to Geophysical Exploration*, 3rd edn., Blackwell Publishing, Oxford, pp. 155–180.

[25] Breiner, S. (1999): *Application Manual for Portable Magnetometer*: Geometrics, California, USA, pp. 1–58.

[26] Riddihoug, R. P. (1971): Diurnal correction to magnetic survey – an assessment of errors: *Geophysical Prospecting*, 19(4), 551–567.

[27] Dobrin, M. B., Savit, C. H. (1988): *Introduction to Geophysical Prospecting*. McGraw-Hill Book Co. Inc., New York, pp. 152–190, 498–578, 691–745.

[28] Nabighian, M. N., Grauch, J. S., Hansen, R. O., LaFehr, T. R., Li, Y., Peirce, J. W., Phillips, J. D. (2005): The historical development of the magnetic method in exploration: *Geophysics*, 70, 33ND–61ND.

[29] Trompat, H., Boschetti, F., Hornby, P. (2003): Improved downward continuation of potential field data: *Exploration Geophysics,* 34, 249–256.

[30] Roest, W. R., Pilkington, M. (1993): Identifying remanent magnetization effects in magnetic data: *Geophysics*, 58, 653–659.

[31] Montaj™ Tutorial. (2004): Two-dimensional frequency domain processing of potential field data.

[32] Akingboye, A. S. (2014): *Geology and Ground Magnetic Investigation over Iron ore deposit, Akunu-Akoko Area Southwestern Nigeria.* Unpublished (BSc.) project, 115 p.

Brought to you by | National Chiao Tung University Library
Authenticated
Download Date | 4/18/17 12:22 PM

Brought to you by | National Technical University of Athens
Authenticated
Download Date | 4/18/17 12:22 PM